Adding Gaussian noise to inaccurate digital elevation models improves spatial fidelity of derived drainage networks

Demetrios Gatziolis and Jeremy S. Fried

Pacific Northwest Research Station, USDA Forest Service, Portland Forestry Sciences Laboratory, Portland, Oregon, USA

Received 20 September 2002; revised 18 November 2003; accepted 26 November 2003; published 26 February 2004.

[1] An economical approach to improving predictions of hydrological models produced highly accurate representations of ephemeral and perennial stream networks. Traditional drainage network extraction from digital elevation models (DEMs) often yields inaccurate and inconsistent results because of elevation errors. Topographic wetness index maps calculated from alternative terrain representations, produced by adding random errors to a DEM of a subwatershed with low relief, were combined to delineate a stream network that matches one produced by more time-intensive (and costly) differential Global Positioning System (GPS) field methods, particularly with respect to the ephemeral component of the drainage network. *INDEX TERMS:* 1848 Hydrology: Networks; 1860 Hydrology: Runoff and streamflow; 1869 Hydrology: Stochastic processes; *KEYWORDS:* digital elevation error (DEM) error, terrain modeling, drainage networks, simulation, wetness index

Citation: Gatziolis, D., and J. S. Fried (2004), Adding Gaussian noise to inaccurate digital elevation models improves spatial fidelity of derived drainage networks, *Water Resour. Res.*, *40*, W02508, doi:10.1029/2002WR001735.

1. Introduction

[2] Delineation of drainage networks remains a fundamental, and still challenging, task in hydrological analysis. Drainage networks are critical in numerous applications, including prediction of flooding and erosion [*Pitlick*, 1994; *Greco*, 1996; *Pilotti and Bacchi*, 1997], modeling of pollution and streamflow dynamics [*Jenson*, 1991], and evaluation of management in the riparian zone [*Bren*, 1995]. Hydrological models that account for the spatial variability of physical properties in a watershed can provide spatially explicit predictions of modeled hydrological variables; however, they require information that defines the internal drainage structure of the watershed, including the drainage network. For example, the ANSWERS [*Beasely et al.*, 1980] and HYDROTEL [*Fortin et al.*, 1995] models require the segments of the watershed's drainage network as inputs. Precise drainage network delineation is increasingly important as land managers seek to achieve fine-grained linking of ground-based measurements of vegetation and remote sensing data to address questions concerning riparian vegetation systems.

[3] Spatially distributed hydrologic models typically rely on digital elevation models (DEMs) to represent terrain as a regular grid (raster) of square, areal elements (cells). The DEMs can be constructed by using a variety of methods. Softcopy photogrammetry on stereo-pairs of digital orthophotos or airborne synthetic aperture radar images is an expensive but relatively precise approach. However, the most common approach relies on digitized contour lines derived from existing topographic maps, such as USGS digital line graph (DLG) files, and the fidelity of the result is determined by contour density [*Gao*, 1997], ratio of contour interval to DEM resolution (cell size), and choice of interpolation algorithm [*Carrara et al.*, 1997]. Accuracy of terrain indices derived from DEMs degrades as contour density and slope decrease, with substantial degradation where slopes are below 5% [*Hammer et al.*, 1995]. Coarse-scale DEMs (i.e., those with large cells) contain less information, generate a smoother-appearing landscape when visualized, and degrade the accuracy of terrain parameters; for example, slope is typically underestimated [*Eash*, 1994]. Most algorithms interpolate elevation between contour lines by fitting a polynomial surface while enforcing monotonic changes in elevation to avoid abrupt slope changes at contour lines. However, they also introduce an artifact of "flattened" elevation values along contours, known as a stair-step effect, which is most pronounced in areas of low relief and leads to increased error in slope predictions computed along contours [*Burrough and McDonnell*, 1998, p. 127]. The stair-step effect is reduced when DEMS are generated by using the ANUDEM algorithm [*Hutchinson*, 1996].

[4] DEMs are widely used for hydrologic modeling, in part because calculation of terrain parameters (e.g., slope, aspect, curvature) and topographic indices (e.g., upslope contributing area, wetness, stream power) is easily accomplished on a raster via directional derivatives. Such parameters can then be processed with algorithms that use map algebra and polynomial or empirical combination, or both, to delineate a spatially explicit drainage network or to calculate topographic indices that correlate with hydrological parameters of interest [*Quinn et al.*, 1995].

[5] Prior to the calculation of topographic indices, depressions (local elevation minima) in a DEM are typically removed to ensure a "depressionless" DEM where all flow paths terminate at the watershed outlet. Although depressions can be real (e.g., in karst or glacial areas), they are rare in DEMs with cell size of 10 m or larger [*Mark*, 1988] and almost always are artifacts introduced during DEM interpolation or reflect positional contour line errors [*Martz and*

0043-1397/04/2002WR001735$09.00

Garbrecht, 1999]. Depression removal entails raising the elevation of all cells in the depression to the elevation of the lowest cell at the depression boundary, a process that produces flat surfaces; or the depression boundary can be breached (lowered) until the depression is furnished with a flow outlet. Pairing the two options can substantially reduce the number and size of filled depressions, especially in low-relief terrain [*Martz and Garbrecht*, 1999].

[6] The most widely used topographic index in hydrological simulations is $\ln(A/S)$, hereafter denoted as topographic wetness index ζ. A is the upslope contributing area, defined as the area drained per unit contour length (or its raster approximation); S is the local slope [*Beven and Kirkby*, 1979]. For a given cell, S is computed as the elevation gradient vector magnitude $|\nabla h|$, where h is the cell elevation value. Note that although an angle is never measured on a DEM directly, S is sometimes referred to as $\tan\beta$, where β denotes the angle between a horizontal plane and a plane tangential to the elevation surface at the cell center. The topographic wetness index value, ζ, is greater for locations that receive runoff from large, upslope areas (e.g., perennial streams) or are relatively flat. In theory, the drainage network can be predicted as locations with index values that are high (e.g., $\geq$95th percentile) relative to the watershed. Such locations are wetter, more likely to reach saturation during rain and snowmelt events, and thus more likely to exhibit infiltration excess overland flow.

[7] ζ is sensitive to the accuracy of calculated slope and to the algorithm used to calculate flow direction, a parameter integral to the computation of A. In the single-flow-direction (deterministic 8-node, also known as D8) algorithm, all flow accumulated upslope of and from a given cell drains to only one of eight neighboring cells, the one with the steepest descent [*O'Callaghan and Mark*, 1984]. Topographic index maps generated by using the D8 algorithm often contain substantial departures from reality and appear inferior to even a casual observer, thanks to the parallel flow artifact, which generates ubiquitous, linear features along only 4 bearings (N/S, NE/SW, E/W, SE/NW). The artifact is less evident in maps generated by using the Rho8 (Random 8-node [*Fairfield and Leymarie*, 1991]) and Frho8 algorithms. Rho8 introduces an aspect-driven modification to D8's flow direction determination. Frho8 furnishes Rho8 with a stochastic component that allows for flow divergence (i.e., routing flow to more than one cell). The random component ensures different results for a given watershed every time Frho8 is applied, which occasionally renders it superior to Rho8. The far more complex digital elevation model networks (DEMON) algorithm represents flow path width, sometimes referred to as stream tube, as constant over planar terrain and increasing/decreasing over divergent/convergent topography to substantially enhance realism [*Costa-Cabral and Burges*, 1994]. Combinations of flow direction algorithms, where algorithm selection is conditioned on local terrain, have emerged in hydrological modeling software packages (e.g., TAPESG [*Moore and Gallant*, 1997]). In a combined approach, algorithms permitting flow divergence are used in the watershed's channel initiation zone (i.e., below a user-defined threshold for upslope contributing area), and are replaced elsewhere by strictly flow-convergent algorithms that better correspond to well-defined drainage networks. The absence of a justifiable, universally applicable method to determine the appropriate threshold for channel initiation, and the likelihood that different thresholds may be better suited to different zones within the same watershed, contribute to an increase in the network's positional uncertainty, at least for network segments of lower order (according to *Strahler*'s [1957] stream segment ordering method).

[8] The effect of algorithm choice on the accuracy of DEM-derived parameters such as A and S has been widely investigated and reported. The elevation errors in a DEM, however, although acknowledged, have received only sporadic attention. In addition to errors introduced during DEM interpolation, elevations stored within digital models contain errors of sampling and measurement [*Fisher*, 1998]. Sampling errors are present at the microterrain scale, where elevation variability within a unit surface areal element represented by a grid cell is collapsed and elevation is reported as being uniform. It is implicitly assumed that the cell value in a DEM is an unbiased estimator of the mean of the elevation value distribution within the area represented by the grid cell. Interpolation and measurement errors produce additional discrepancies between the true mean elevation for a grid cell and the one reported in the DEM. If the true mean elevation of a grid cell with coordinate vector at its center $\mathbf{u} = (x, y)$ is $h(\mathbf{u})$, and $d(\mathbf{u})$ is the corresponding DEM value, then the discrepancy, or error, $\epsilon(\mathbf{u})$ is defined as

$$\epsilon(\mathbf{u}) = h(\mathbf{u}) - d(\mathbf{u}) \tag{1}$$

although both $h(\mathbf{u})$ and $\epsilon(\mathbf{u})$ are unknown, often some information is available on the distribution of the latter. This type of information can best be used by representing it as a random variable $E(\mathbf{u})$ [*Heuvelink*, 1998, p. 9]. Although it is obvious that mean elevation at location $\mathbf{u}$ has only one, true, deterministic value, $h(\mathbf{u})$, the uncertainty about $h(\mathbf{u})$ allows treating it as a random variable, $H(\mathbf{u})$, affected by the sampling, measurement, and interpolation mechanisms mentioned previously. Therefore the error model in (1) becomes

$$H(\mathbf{u}) = d(\mathbf{u}) + E(\mathbf{u}), \forall \mathbf{u} \in D \tag{2}$$

where D, the planar extent of the DEM in question, is a subset of the two-dimensional space R^2. An elevation surface $H(\cdot) \equiv \{H(\mathbf{u})|\mathbf{u}\in D\}$ and the corresponding error surface $E(\cdot) \equiv \{E(\mathbf{u})|\mathbf{u}\in D\}$ can be thought of as large sets of random variables, although in the geostatistical literature, these surfaces would be described as random fields, or random functions [*Cressie*, 1991]. The error random variables $E(\mathbf{u})$ in (2) are assumed to follow a Gaussian distribution. The implication of (2) is that a DEM can be regarded as a realization generated from sampling the error distributions associated with each of its cells, and that alternative realizations from the population of $E(\cdot)$ can be generated, were the latter to be known.

[9] Recent investigations have revealed that $E(\cdot)$ exhibits spatial autocorrelation and anisotropy, tends to cause elevation underestimation in ridges, and overestimation in valleys [*Liu and Jezek*, 1999], and it is positively correlated with slope [*Hunter and Goodchild*, 1997; *Veregin*, 1997]. Where high-accuracy elevation observations $h(\mathbf{v})$ are available at discrete points $\mathbf{v} = (x, y)$ for a DEM (e.g., from field surveys

or high-resolution DEMs), $\epsilon(\mathbf{v})$ can be computed from (1), and the covariance between $h(\mathbf{v})$ and $\epsilon(\mathbf{v})$ [i.e., $\mathrm{cov}\{h(\mathbf{v}), e(\mathbf{v})\}\forall\mathbf{v}$] can be estimated. Geostatistics can then be employed to provide locally conditioned, DEM-wide estimates of elevation error [*Kyriakidis et al.*, 1999]. Resulting models of elevation uncertainty allow generation of alternative elevation realizations that preserve the elevation values $h(\mathbf{v})$ and the local covariance structure $\mathrm{cov}\{h(\mathbf{v}), e(\mathbf{v})\}$ for the known locations and also estimate the elevation values $h(\mathbf{u})$ for all the unsampled locations via stochastic simulation [*Goovaerts*, 1997]. In the absence of high-accuracy elevation measurements (the usual case) and where only a global estimate of root mean square elevation error (RMSE) is available, such as in USGS DLGs and DEMs, the error is assumed stationary and isotropic. In such a case, $\mathrm{cov}\{h(\mathbf{u}), \epsilon(\mathbf{u})\} = 0$, $\mathrm{var}(\epsilon(\mathbf{u})) = \mathrm{RMSE}^2$, and $\mathrm{cov}\{e(\mathbf{u}), e(\mathbf{u} + \mathbf{x})\} = C_\epsilon(x), \forall\mathbf{u}, (\mathbf{u} + x)\in D$, where $x = |\mathbf{x}|$, and $\mathbf{x}$ is the separation (lag) distance vector. Error realizations can initially be generated by drawing values from a standard Gaussian distribution with zero mean and standard deviation equal to the reported RMSE [*Goodchild*, 1980; *Fisher*, 1991]. Because the error realizations thus generated exhibit abrupt value changes between adjacent cells, the random error values are repeatedly swapped until a target autocorrelation, typically measured by the Moran's or Geary's index, is achieved. Alternatively, the random error values are convolved with adjacent values to produce correlated error realizations [*Ehlschlaeger et al.*, 1997]. In both approaches, the targeted autocorrelation, a function of covariance structure $C_\epsilon(x)$, is chosen arbitrarily because although the moments of the error distribution are assumed to be known, $C_\epsilon(x)$ is not. In the convolution approach, $C_\epsilon(x)$ is related to the structure of the convolution filter employed.

[10] The assumption of nonstationary DEM error, generally appropriate for watersheds of rugged terrain [*Hunter and Goodchild*, 1997; *Kyriakidis et al.*, 1999] can potentially be relaxed for watersheds with very gentle terrain. Recent investigations involving stochastic simulation of DEM error in a watershed with rugged terrain (elevation range >800 m, mean slope 10.7 degrees) found little association between the spatial distribution of elevation error and computed terrain attributes [*Holmes et al.*, 2000]. Thus ζ may be little affected by DEM error nonstationarity, even in rugged terrain watersheds. And, given the positive correlation between elevation error and slope found in other studies [e.g., *Veregin*, 1997], one would expect even less influence of DEM error nonstationarity on terrain indices in watersheds with low slope and low slope variability, lending support for the assumption of DEM error stationarity in gentle terrain watersheds.

[11] Elevation errors in a DEM propagate through terrain parameter calculation [*Lagacherie et al.*, 1996] to compromise the accuracy of hydrological simulations and computed topographic indices [*Walker and Willgoose*, 1999]. The effect of elevation error on distributed topographic indices can be estimated in a Monte Carlo framework in which simulated DEM surfaces are obtained by adding an elevation error surface [*Heuvelink*, 1998, p. 78] to an existing DEM to relate uncertainty of topographic indices to elevation uncertainty; such information can be useful for assessing the utility of decision-support models that incorporate topographic indices.

[12] In this paper, we investigate via simulation the effect of intentionally introduced DEM errors on the delineation of the drainage network for a small subwatershed with very gentle, rolling terrain. We assumed that (1) elevation errors are spatially structured but that autocorrelation is independent of watershed location and (2) error distribution parameters reported for the elevation contour representation (USGS DLG) approximate those for the contour-generated DEM. Drainage network realizations derived from both the original DEM and simulated terrain are compared to a realization generated from field observations.

2. Methods

2.1. Study Area and DEM Generation

[13] The 4.7 km^2 Barnard Drain subwatershed selected for this study is part of the Sycamore Creek Watershed, located just south of the city of Mason in Ingham County, Michigan. Row crops and forests are the most common land use/cover accounting for 80% and 15% of the subwatershed area, respectively. Capac and Marlette fine sand loams are the dominant soil types, representing 82% and 11% of the subwatershed, respectively [*U.S. Soil Conservation Service*, 1979]. A 10-m DEM for Barnard Drain was generated from a 1:24,000 USGS digital hypsography (contour line) coverage (Figure 1a). The DEM was generated with the ESRI ArcInfo TOPOGRID function that implements *Hutchinson*'s [1989] algorithm by using default tolerances for sink removal. The 10-m DEM cell size was selected because it is comparable to the width of perennial streams in this landscape. Slope percentages calculated from the DEM via finite differences, are very gentle (maximum 12.8, mean 1.9, standard deviation 1.6).

[14] The perennial and ephemeral drainage network, defined as the locus of points where observers either detected evidence of surface runoff or witnessed overland flow during, or immediately after, rainfall events, was georeferenced by a Global Positioning System (GPS) receiver and stored as a vector coverage containing 9144 m of ephemeral and 3425 m of perennial streams. The vector coverage was converted to a 10-m grid (T_{obs}) with the same spatial extent as the DEM, and

$$T_{obs} = \left\{ \begin{array}{ll} 1, \text{ if } \mathbf{u} \text{ contains an observed drainage network segment} & \\ & \forall\mathbf{u} \in D \\ \text{Null otherwise} & \end{array} \right\} \quad (3)$$

[15] Because a paucity of locations with precisely known elevations in the study area precluded direct assessment of DEM accuracy, an indirect approach was used. Fifty locations distributed across the subwatershed were precisely georeferenced (in two-dimensional space) by using GPS. Horizontal precision achieved with local benchmarks averaged 0.58 m. For each location, the sign of elevation difference relative to all other GPS-surveyed locations within 100m was assessed with a tripod-mounted clinometer, generating 182 observations of relative elevation difference. In only 79% of these cases did the sign of the observed difference match that computed from the DEM. Sign disagreement was more frequent in areas with minimal slope. The lack of absolute elevation information for these

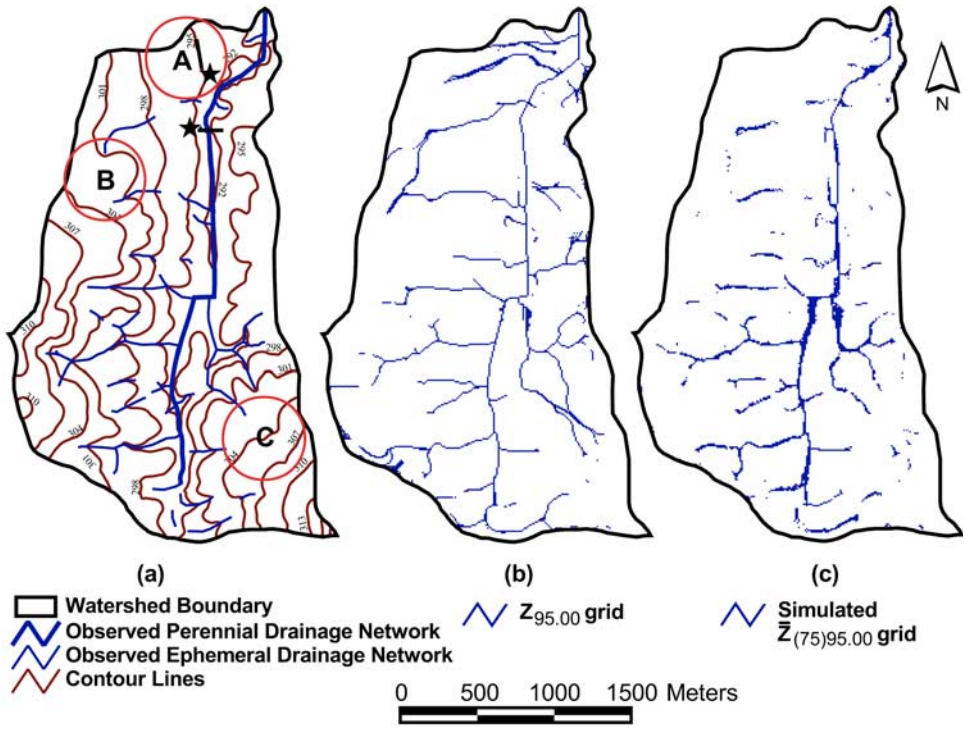

Figure 1. (a) Observed perennial and ephemeral drainage network, hypsography, and areas of low contour density (lettered circles) for Barnard Drain subwatershed. Stars denote locations analyzed to evaluate performance of the model. (b) Topographic wetness index 95th percentile grid calculated with the D8 flow-routing algorithm on a DEM generated from a 1:24,000 USGS DLG. (c) Mean topographic wetness index 95th percentile grid, calculated using the D8 flow-routing algorithm on 75 DEM realizations, produced by using a 100-m radius Gaussian elevation error processing kernel.

50 locations precluded estimation of the elevation error covariance per lag distance $C_\epsilon(x)$.

[16] Map accuracy standards require that for 90% of distinguishable features, DLG-reported elevation be within half a contour interval (±5 feet in the case of 1:24,000 USGS DLG) of the true (error-free) feature elevation [*U.S. Bureau of the Budget*, 1947]. For a Gaussian distribution with mean 0 and a 90% confidence interval extending from −1.524 to 1.524m (plus or minus half of one 10-ft DLG contour interval), the corresponding RMSE equals 0.929m. Random grids (for a spatial extent set to that of the DEM plus a 150-m buffer and a cell size identical to that for the DEM) were generated by using these distribution parameters ($N \sim (0, 0.929)$). The buffer zone was used to eliminate edge effects during grid smoothing (to be discussed shortly), and was subsequently removed.

[17] Random grids lack spatial structure (i.e., no autocorrelation). The ''surface'' they represent is discontinuous, has abrupt value changes between adjacent cells, abundant local minima (sinks) and maxima, and is unsuitable for terrain modeling. Autocorrelation is introduced with grid processing of a kernel window. The size of the window (K_i, measured in cells) controls the smoothing intensity (larger windows provide more smoothing), and hence the level of autocorrelation. Circular kernels with radii of 50, 100, and 150 m were used to introduce varying degrees of autocorrelation. Because the kernel application on the random grids reduces the standard deviation of cell values proportionally to the square root of the kernel window size [*Heuvelink*, 1998, p. 46], cell values were multiplied by $\sqrt{K_i}$ to restore the targeted value of standard deviation. Note that a scalar multiplication does not affect autocorrelation. Moran's *I* correlation coefficients [*Moran*, 1950; *Bailey and Gatrell*, 1995, p. 270], calculated as function of distance (lag) on the kernel-processed random grids are shown in Figure 2. *I* values were calculated for individual 10-m lag increments so that a coefficient pertaining to a larger lag would not be partially influenced by grid autocorrelation at smaller lags. For the benefit of the reader more familiar with variograms than Moran's *I*, empirical variograms for the kernel-processed random grids are superimposed in Figure 2. It is easy to see that the spatial extent of autocorrelation equals the diameter of corresponding kernel. Note that kernels of smaller radius, and hence weaker autocorrelation generators, were not considered because when the smoothed random grids they produce are added to the DEM, the resulting surface realizations still contain a large number of sinks. Elimination of those sinks, necessary in subsequent analysis stages, would have resulted in excessive surface terracing, which tends to inflate ζ values. Larger kernel radii were also rejected because they were found to produce a practically flat error surface. Application of the selected kernels served to convert the random grids to autocorrelated elevation error surfaces.

2.2. Generation and Processing of Topographic Wetness Index Grids

[18] Elevation realizations produced by adding these autocorrelated error surfaces to the original DEM contained

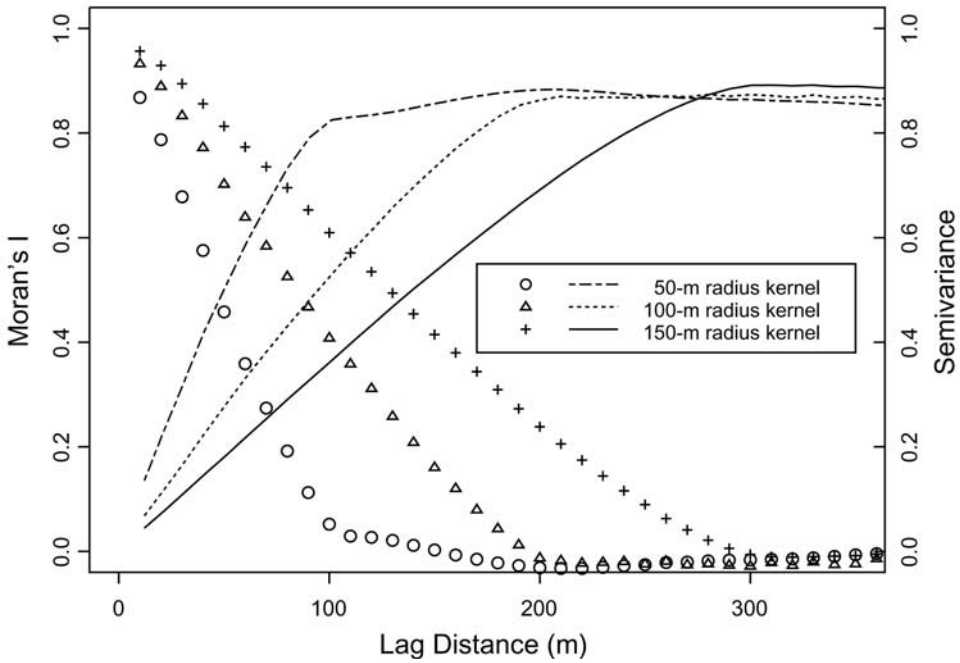

Figure 2. Moran's *I* correlation coefficients and empirical variograms calculated at 10-m lag distance increments from 10-m elevation error surface generated by using circular kernels with radii of 50 m, 100 m, and 150 m. Symbols represent Moran's *I*. Empirical variograms calculated at discrete intervals are presented as lines for visualization purposes.

a number of sinks formed where the error surface introduced narrow bands of cells of higher elevation across convergent flow paths. Sinks of such nature were identified and their boundaries were, depending on their horizontal and vertical magnitude, either breached or lowered. Remaining sinks were eliminated in the conventional manner by sink filling. Sink identification and processing was implemented by using the Topographic Parameterization (TOPAZ) software package [*Agricultural Research Service*, 2000].

[19] Local slope, S, estimates were obtained from the elevation realizations prior to sink processing to minimize the number of cells situated at flat spots where $1/S$ is undefined. S was calculated with the finite differences algorithm [*Wilson and Gallant*, 2000, p. 52]; local drainage direction and A were estimated from the sink-free elevation realizations. Spatially distributed estimates of the topographic wetness index, ζ were calculated by using both D8 and DEMON drainage direction (flow-routing) algorithms to produce grids of topographic wetness index, denoted henceforward by Z. All parameters were computed by using the Terrain Analysis Programs for the Environmental Sciences Grid version (TAPESG); chapter 3 of *Wilson and Gallant* [2000] provides detailed descriptions of these algorithms and their performance.

[20] A total of six Z-grid sets, each containing 180 realizations, were simulated by using three smoothing-kernel radii (50, 100, 150 m) and the two flow-routing algorithms (D8, DEMON). To assess the effect of simulation intensity (defined as the number of Z realizations generated and averaged to produce a mean Z-grid) on topographic wetness index, the 180 Z-grid realizations in each set were randomly assigned to six groups, with memberships, k, of 5, 10, 15, 25, 50, and 75 grid realizations. For each group within a set, the mean Z grid ($\overline{Z}_{(k)}$) was calculated as

$$\overline{Z}_{(k)} \equiv \left\{ \overline{\zeta}_{(k)}(\mathbf{q}) = \frac{1}{k} \sum_{i=1}^{k} \zeta_i(\mathbf{q}), \forall \mathbf{q} \in \mathrm{D} \right\}, \tag{4}$$

where $\zeta_i(\mathbf{q})$ is the value of grid Z_i of a given group at grid cell location $\mathbf{q}$. Further, percentile values ζ_λ, λ taking values 92.50, 95.0, 96.29, and 97.50, were determined from the distribution of cell values within each $\overline{Z}_{(k)}$. Percentile 96.29 was chosen because it corresponds to the number of cells in the grid representing the field observed drainage network, T_{obs}. The ζ_λ values were used to produce unit-value reclassification grids $\overline{Z}_{(k)\lambda}$ for each $\overline{Z}_{(k)}$, with

$$\overline{Z}_{(k)\lambda} \equiv \left\{ \begin{array}{l} 1, \text{if } \overline{\zeta}_{(k)}(\mathbf{q}) \geq \zeta_\lambda \\ \\ \text{Null otherwise} \end{array} , \forall \mathbf{q} \in \mathrm{D} \right\} \tag{5}$$

The cells in each $\overline{Z}_{(k)\lambda}$ grid with a value of 1 have the highest average wetness index values in the subwatershed; thus these grids represent predicted drainage networks, and the cells with value equal to 1 are henceforth referenced as "wet."

2.3. Comparison Between the Observed and Simulated Drainage Network

[21] Assessing the degree of spatial cooccurrence between T_{obs} and each $\overline{Z}_{(k)\lambda}$ calls for a quantitative approach. Although visual evaluations can provide a useful first approximation, they are not well suited to detecting small differences, such as those produced by incremental changes in simulation intensity k and may be difficult to

apply repeatedly. Other studies have relied on statistical methods to provide quantitative evaluation, but these usually operate on parameters that characterize aggregate simulation output (total stream length, stream segment order, etc.) and omit the spatial component from the comparison.

[22] A measure of spatial cooccurrence, Φ, should be sensitive to both errors of omission (i.e., where a segment of observed drainage network is not colocated with a segment of predicted network), errors of commission (i.e., where a segment of predicted network is not colocated with a segment of the observed drainage network), and account for the magnitude of the positional discrepancy, if any. In addition, Φ should not be sensitive to the length of observed and predicted drainage network, so that simulation outputs resulting in different predicted network lengths can be compared. An intuitive metric for discrepancy quantification is the Euclidean distance between observed and predicted network segments. The metric could be applied directly if for a given "wet" cell in, for example, T_{obs}, a unique, corresponding "wet" cell in $\overline{Z}_{(k)\lambda}$ could be identified. However, even where predicted network segments correspond to observed network segments, they rarely have identical shapes or cell membership. Therefore Euclidean distance is only indirectly useful.

[23] For each "wet" cell in T_{obs}, we calculated the Euclidean distance to the nearest "wet" cell in $\overline{Z}_{(k)\lambda}$ as the distance between the cell centers. Summing these distance values and normalizing by the number of "wet" cells in T_{obs} produced the scalar cooccurrence omissions component Φ_o, a weighted average of the positional discrepancy of T_{obs} from $\overline{Z}_{(k)\lambda}$. For each "wet" cell in $\overline{Z}_{(k)\lambda}$, we calculated the Euclidean distance to the nearest "wet" cell in T_{obs}, then summed these distance values and normalized by the number of "wet" cells in $\overline{Z}_{(k)\lambda}$ to produce the scalar cooccurrence commissions component Φ_c, a weighted average of the positional discrepancy of $\overline{Z}_{(k)\lambda}$ from T_{obs}. Assuming that errors of commission are as equally important as errors of omission, the two weighted averages can be added to produce Φ.

[24] Φ_o and Φ_c are disproportionately influenced by the presence of small clusters of cells in the observed or predicted network located far from the predicted and observed network, respectively. This weakness can be overcome by truncating the distance value. Both an upper and a lower distance truncation threshold were imposed. The lower threshold was arbitrarily set at 10m (one cell). This threshold normalizes the influence on Φ of the positional uncertainty introduced during the conversion of the observed drainage network from line (vector) to areal (grid) form. While all cells containing a segment of the observed network are characterized as "wet" in T_{obs} (equation (3)), it is quite likely that many null cells in T_{obs} that are very close to a segment of the observed network vector coverage (and adjacent to cells in T_{obs} classified as wet) likely contain portions of the drainage network. The use of a lower distance threshold equates such null cells to wet cells for the purpose of computing Φ_o. For consistency, the lower threshold is also used in computing Φ_c.

[25] Subsequently, iteratively increasing (by 10 m) the distance truncation threshold value and statistically comparing the distance value frequency distributions prior to and after truncation identified the appropriate upper threshold. The latter was set as the smallest truncation distance for which the null hypothesis of equal distance value frequency distributions prior to and after truncation could not be rejected. The statistical testing was performed by using the Pearson's rank correlation with $\alpha = 0.95$, because the absence of normality in both the pretruncation and post-truncation frequency distributions precluded the use of a parametric statistical test. Given that a total of 144 $\overline{Z}_{(k)\lambda}$ grids were computed (6 choices for k, 4 for λ, 2 for D8/DEMON, and 3 for kernel radii) the statistical test was repeated in 288 iterations; 144 times on the distance distributions of $\overline{Z}_{(k)\lambda}$ from T_{obs} and 144 times on distance value distribution of T_{obs} from each $\overline{Z}_{(k)\lambda}$. In all but 5 iterations the appropriate truncation threshold was found to be 60 m. For 4 iterations ($\overline{Z}_{(10)92.50}$ calculated with D8 and 150 m kernel, $\overline{Z}_{(15)97.50}$ calculated with DEMON and 150 m kernel, $\overline{Z}_{(5)96.29}$ calculated with D8 and 100 m kernel, and $\overline{Z}_{(15)95.00}$ calculated with D8 and 50 m kernel) it was 50 m, and for one ($\overline{Z}_{(15)95.00}$ calculated with DEMON and 100 m kernel) it was 70 m.

[26] After identifying the appropriate truncation distance, the distance grids ΔT_{obs} and $\Delta\overline{Z}_{(k)\lambda}$ for a T_{obs}, $\overline{Z}_{(k)\lambda}$ pair were defined as

$$\Delta T_{obs} = \begin{cases} 60, & \text{if } \vartheta\left(\mathbf{u}, \overline{Z}_{(k)\lambda}\right) > 60 \\ \vartheta\left(\mathbf{u}, \overline{Z}_{(k)\lambda}\right), & \text{if } 10 \le \vartheta\left(\mathbf{u}, \overline{Z}_{(k)\lambda}\right) \le 60 \\ 10, & \text{if } \vartheta\left(\mathbf{u}, \overline{Z}_{(k)\lambda}\right) < 10 \end{cases} \quad \forall\left[\mathbf{u} \in T_{obs} \mid t(\mathbf{u}) = 1, \; \mathbf{q} \in \overline{Z}_{(k)\lambda} \mid \overline{\zeta}_{(k)\lambda}(\mathbf{q}) = 1\right] \tag{6}$$

and

$$\Delta\overline{Z}_{(k)\lambda} \equiv \begin{cases} 60, & \text{if } \vartheta(\mathbf{q}, T_{obs}) > 60 \\ \vartheta(\mathbf{q}, T_{obs}), & \text{if } 10 \le \vartheta(\mathbf{q}, T_{obs}) \le 60 \\ 10, & \text{if } \vartheta(\mathbf{q}, T_{obs}) < 10 \end{cases} \quad \forall\left[\mathbf{q} \in \overline{Z}_{(k)\lambda} \mid \overline{\zeta}_{(k)\lambda}(\mathbf{q}) = 1, \; \mathbf{u} \in T_{obs} \mid t(\mathbf{u}) = 1\right] \tag{7}$$

where $\vartheta(\mathbf{r}, B)$, is a function that calculates the Euclidean distance between a point at location $\mathbf{r}$ (grid cell center) and the closest point in a set of points (grid cell centers) B, $B = \{\mathbf{b_1}, \mathbf{b_2}, \ldots, \mathbf{b_N}\}$. Hence

$$\vartheta(\mathbf{r}, B) = \min \parallel \mathbf{r} - B \parallel, \forall \mathbf{b} \in B. \tag{8}$$

$t(\mathbf{u})$ denotes the value of T_{obs} at location $\mathbf{u}$, $\overline{\zeta}_{(k)\lambda}(\mathbf{q})$ denotes the value of $\overline{Z}_{(k)\lambda}$ at location $\mathbf{q}$, while $t(\mathbf{u}) = 1$ and $\overline{\zeta}_{(k)\lambda}(\mathbf{q}) = 1$ represent "wet" cells of T_{obs} and $\overline{Z}_{(k)\lambda}$ at locations $\mathbf{u}$ and $\mathbf{q}$ respectively. The positional discrepancy Φ for a T_{obs}, $\overline{Z}_{(k)\lambda}$ pair was calculated as

$$\Phi = \Phi_o + \Phi_c = \frac{\sum t(\mathbf{u})}{Nt} + \frac{\sum \overline{\zeta}_{(k)\lambda}(\mathbf{q})}{N\overline{\zeta}}, \quad \forall\left[\mathbf{u} \in \Delta T_{obs}, \mathbf{q} \in \Delta\overline{Z}_{(k)\lambda}\right] \tag{9}$$

where Nt represents the number of grid cells in ΔT_{obs} and $N\overline{\zeta}$ represents the number of grid cells in $\Delta\overline{Z}_{(k)\lambda}$. Note that for a given level of fidelity in the predicted drainage network, as λ increases, $N\overline{\zeta}$ becomes smaller and $\sum t(\mathbf{u})$ tends to decrease, while $\sum\overline{\zeta}_{(k)\lambda}(\mathbf{q})$ tends to increase (the latter because of a lower frequency of short distance values in $\Delta\overline{Z}_{(k)\lambda}$). It is evident from (9) that an increase in λ, tends to decrease Φ_o and increase Φ_c. Adding Φ_o and Φ_c to create

Φ nearly equalizes the trends and results in a robust statistic across a range of λ values.

[27] Φ can alternatively be computed just for the perennial, Φ_{per}, or ephemeral Φ_{eph} components of the drainage network. However, the computation of Φ_{per} and Φ_{eph} necessitates labeling the "wet" grid cells in $\overline{Z}_{(k)\lambda}$ as either ephemeral or perennial, a distinction that is known a priori in T_{obs}. We labeled members of the simulated perennial drainage network the "wet" grid cells included in a two-cell buffer built around the observed drainage network. Isolated grid cells of the simulated network within the buffer and all those outside the buffer were labeled members of the ephemeral network.

[28] A perfect spatial correspondence between T_{obs} and $\overline{Z}_{(k)\lambda}$ grids would produce an optimum (smallest) Φ of 20, because, as implied by (6) and (7), 10 is the minimum that could be assigned to each of Φ_o and Φ_c, Φ's components. An optimum Φ of 20 would hold for most realistic choices of the percentile threshold, λ, that result in a predicted drainage network longer or shorter than the observed network. This property of Φ results from the provision for a lower distance truncation threshold in equations (6) and (7), which generates single-cell buffers with cell-value of 10 around each wet cell in ΔT_{obs} and $\Delta\overline{Z}_{(k)\lambda}$. The number of cells in these buffers would be, for most drainage network configurations, large enough to host either a. the number of wet cells in $\Delta\overline{Z}_{(k)\lambda}$ in excess of the number of wet cells in ΔT_{obs} where the choice of λ results in $N\overline{\zeta} > Nt$, or b. the number of wet cells in ΔT_{obs} in excess of the number of wet cells in $\Delta\overline{Z}_{(k)\lambda}$ where the choice of λ results in $N\overline{\zeta} < Nt$. Hence occurrences of spatial discrepancies between T_{obs} and $\overline{Z}_{(k)\lambda}$ strictly due to differences between Nt and $N\overline{\zeta}$ would not inflate the optimum value of Φ. In the absence of a lower distance truncation threshold, the optimum Φ would be 0 when $Nt = N\overline{\zeta}$, and greater than 0 for every choice of λ that results in $Nt \neq N\overline{\zeta}$. In addition, an optimum Φ of 0 would preclude meaningful evaluation of percentage change in Φ associated with alternative simulation scenarios.

3. Results

[29] The spatial fidelity of the derived drainage network, as represented by Φ, was controlled (in decreasing degree) by simulation intensity k, choice of flow-routing algorithm, percentile λ used for computing $\overline{Z}_{(k)\lambda}$, and level of autocorrelation for the elevation error surface. Even light simulation intensity (e.g., 5 and 10 topographic wetness index realizations) considerably improved network fidelity compared to the fidelity of the network derived from the unperturbed DEM (Figure 3). The incremental gain in fidelity decreased with progressively larger simulation intensity and reached asymptotes between 50 and 70 realizations for D8 and 25 and 40 for DEMON; Φ had practically the same asymptote value with both algorithms. It was only marginally smaller when the 100-m radius was used for error surface generation, compared to when 50-m and 150-m radii were used (Figure 4). Spatial autocorrelation of elevation error had minimal effect on the fidelity of the drainage network. Realizations generated by using the 100-m kernel yielded slightly better (smaller) values for Φ.

[30] Deterministic Φ values (i.e., without elevation error simulation) were better (lower) for larger λ ("Det" in Figure 3). Lowering the percentile increased the ratio of the predicted ephemeral to total drainage network length and monotonically inflated Φ. With elevation error simulation, Φ improvement for large λ (e.g., 97.50) was much weaker than for smaller (96.29 or 95.00) percentiles, an observation suggesting that elevation error simulation primarily benefited the representation fidelity of the ephemeral network. Across percentiles, there was practically no difference in the representation fidelity of the perennial drainage network, although fidelity varied remarkably for the ephemeral network (Figure 5). Φ_{per} computed for the unperturbed DEM using the D8 algorithm (Figure 1b) was 24.11, similar to the value obtained using the same algorithm, and 75 elevation realizations (Figure 5). Φ_{eph} computed for the unperturbed DEM however, was 58.62, much larger than the Φ_{eph} computed for any of the simulated ephemeral drainage networks (Figure 5).

[31] Interesting insights regarding the performance of our approach for drainage network delineation are gained by examining the per cell ζ distribution moments derived from elevation realizations along two transects within the subwatershed, and then contrasting them with deterministic ζ values computed on the original DEM. The first transect is positioned orthogonal to the flow direction of the perennial stream and the second orthogonal to the gradient of local slope (and parallel to contours). Transects are star-marked in Figure 1a. Where topography is well defined, the introduction of elevation error of a magnitude expected to be present in USGS DLG-derived DEMs only marginally affects the delineation of the drainage network. The 15-cell transect across the perennial network shows a cell (8) as member of the network in both deterministic and simulated network derivation approaches (Figures 6a and 6c). The cell's ζ_{det} (diamonds in Figure 6) and $\overline{\zeta}_{(75)}$ (short, thick lines) values are larger than the critical global values $\zeta_{det,95.00}$ and $\overline{\zeta}_{(75),95.00}$ (horizontal dashed lines), and therefore are considered members of the predicted deterministic and simulated networks respectively. Transect cell 7 though is also predicted as member of the network in the deterministic approach (diamond above the $\zeta_{det,95.00}$ dashed line) but not in the simulated (thick line below the $\overline{\zeta}_{(75),95.00}$ dashed line). In this case, simulation helps thin the network width from two cells to one, and field observations confirmed that the simulated result better reflects reality for that location. Note that transect cells 7 and 8 have a much wider ζ range (as shown by whiskers) because of a few extreme values originating from simulated flow concentration either occasionally passing through the cell (7) or missing it (8). For both cells though, the narrow range between the 25th and 75th percentile of ζ value distribution leaves little doubt that cell 8 is network member whereas cell 7 is not. Note that transect cells 5 and 6 correspond to a local elevation maximum adjacent to Barnard Drain. Their narrow range and very low $\overline{\zeta}_{(75)}$ demonstrate that elevation error simulations do not eliminate local maxima.

[32] Where topography is more ambiguous (e.g., areas that are flat or characterized by straight and widely separated, parallel contour lines as shown in circles A, B, and C in Figure 1a), even small elevation changes alter the computed flow direction and A and hence generate a wide range of ζ values. Owing to highly variable flow routing among multiple elevation realizations for most flat

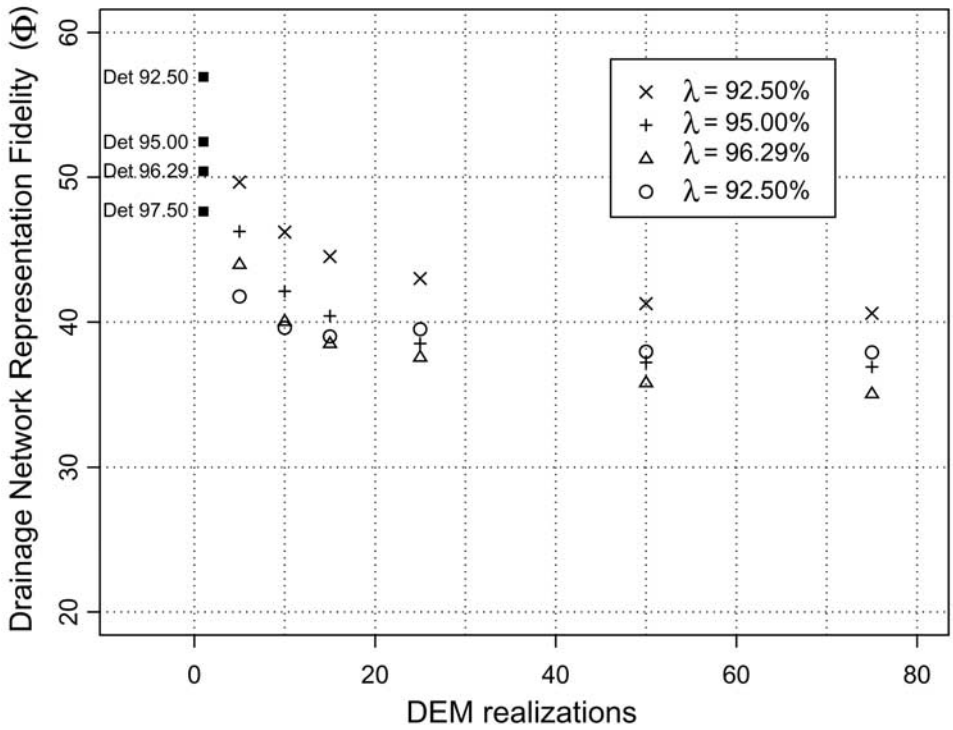

Figure 3. Representation fidelity (expressed via the Φ statistic) of drainage network derived from modeling elevation error on a 10-m DEM generated for the Barnard Drain subwatershed in Ingham County, Michigan, from a 1:24,000 USGS DLG by using the D8 flow-routing algorithm and a 100-m kernel window, plotted as a function of the number of DEM realizations for selected and topographic wetness index value percentiles (λ). Squares represent deterministic ("Det") Φ statistic values obtained from the unperturbed DEM for selected percentiles.

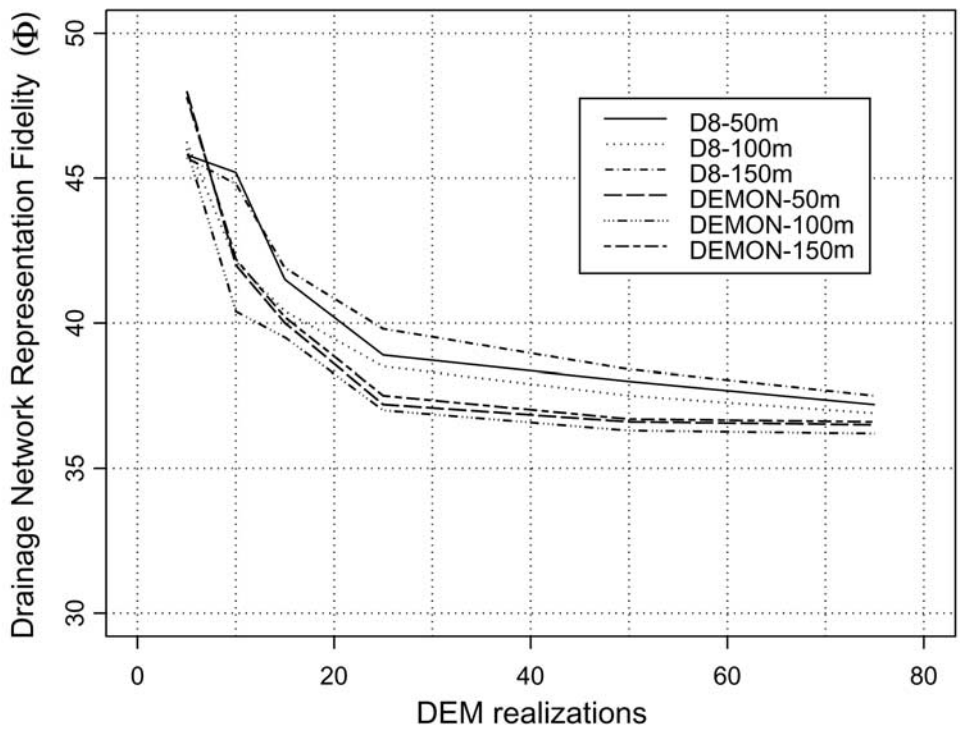

Figure 4. Representation fidelity (expressed via the Φ statistic) of drainage network derived from modeling elevation error as a function of the number of DEM realizations for two flow-routing algorithms (D8 and DEMON), three kernel radii (50, 100, and 150 m), and topographic wetness index value percentile (λ) of 95.

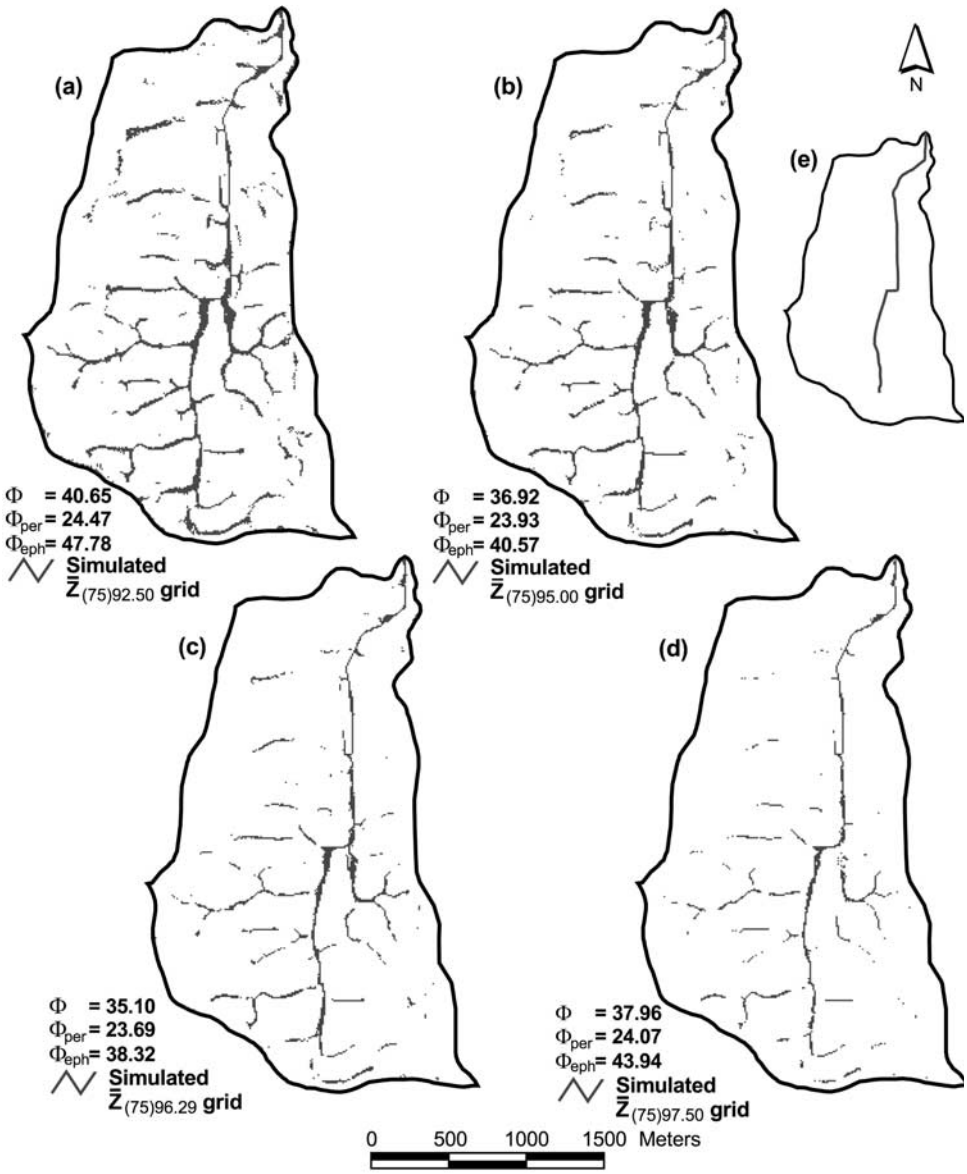

Figure 5. (a–d) Mean topographic wetness index percentile grids and predicted drainage network representation fidelity statistics (overall, Φ, of perennial network, Φ_{per}, and of ephemeral network, Φ_{eph}) calculated by using the D8 flow-routing algorithm on 75 DEM realizations produced by using a 100-m radius Gaussian elevation error processing kernel. (e) Observed perennial drainage network.

areas, the corresponding $\bar{\zeta}_{(k)}$ values for all cells in these areas rank consistently well below the global $\bar{\zeta}_{(k),\lambda}$ threshold. The ζ distribution moments for the second 15-cell transect (Figures 6b and 6d), shows no cells being members of the simulated network (the actual case) for both D8 and DEMON modeling. The deterministic approach shows 2 cells when DEMON is used and 4 cells when D8 is used as network members. The deterministic topographic wetness index calculation over ambiguous terrain demonstrates DEMON's sensitivity in flow convergence/divergence. Cells along the transect show gradual change in $\zeta_{det,95.00}$ using the DEMON but abrupt changes when using the D8 (Figures 6b and 6d). In ambiguous terrain, deterministic applications of D8 often perform poorly; however, even moderate simulation intensity largely overcomes this limitation.

[33] The DEMON algorithm was nearly twice as efficient as D8 in delineating the drainage network in terms of the number of elevation realizations required to reach a Φ asymptote. This performance is likely due to DEMON's ability to expand/contract flow paths over divergent/convergent topography. Although the advantage of such flexibility likely would diminish with increasing elevation error and decreasing autocorrelation, it conferred clear superiority for the elevation error patterns reported by USGS DLG metadata. However, DEMON is computationally intensive. In our application it required approximately four times more computation time per elevation realization processing than D8. In addition, for a given DEM resolution, computation time and computing resources (e.g., RAM) required by DEMON increases exponentially with watershed size. Thus, although D8 requires a larger number of elevation realiza-

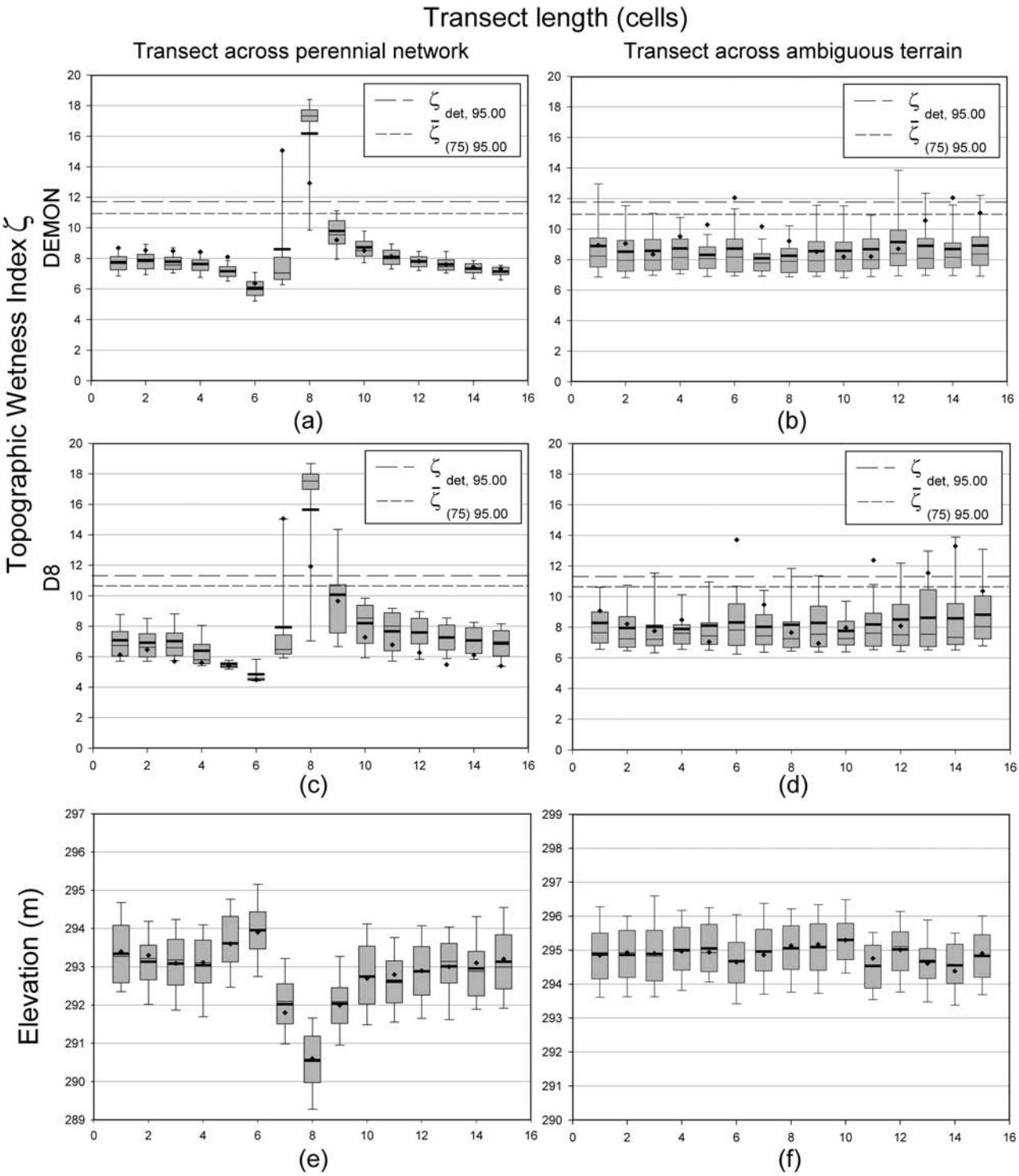

Figure 6. Topographic wetness index deterministic values (from the unperturbed DEM) and distribution moments calculated for two 15-cell transects from 75 elevation realizations generated by using 100-m elevation error smoothing kernel and the 95th mean topographic wetness index reclassification percentile and perturbed/unperturbed transect elevation. Distribution moments symbolization is as follows: Thick line, mean; thin line, median; shaded box, 25th to 75th percentile; upper/lower whisker, 90th/10th percentile. Diamonds denote deterministic values. Dashed horizontal lines represent global 95th percentile mean topographic wetness index percentile values calculated deterministically and for 75 elevation realizations. Diamonds in Figures 6e and 6f denote unperturbed elevation. Elevation variability was calculated prior to hydrologic processing of the DEM.

tions to achieve drainage network delineation of comparable quality, it likely will be preferred where computation time is critical.

[34] The very limited information on the error available in USGS DLG maps and DEMs, in most cases a single, nonspatial, RMSE estimate, precludes an assessment of the error's covariance structure. In the interest of using this limited information for improved terrain attribute and index estimation, and in the absence of other accurate elevation information, as it is usually the case, there is no choice other than arbitrarily selecting an error covariance structure, and hence autocorrelation. In our application we introduced autocorrelation by processing random grids with circular kernels of various radii, thus selecting, albeit implicitly, a kernel-size-related covariance structure (Figure 2). Obviously, other covariance structures could be used either via different kernel structures or explicitly with well-established autocorrelation generators such as the sampling from the spectrum or turning bands methods [*Mejia and Rodriguez-Iturbe*, 1974; *Mantoglou and Wilson*, 1982] to name a few.

[35] A limited range of options is available for defining covariance structures of autocorrelated error surfaces to be added onto existing DEMs to produce elevation realizations for hydrological modeling because, unlike other studies involving error surfaces, in hydrological modeling each elevation realization is further processed for sink elimination (often referred to as drainage enforcement). If an error surface with weak autocorrelation is added onto a DEM representing a gentle terrain watershed, and the elevation realization is processed for sink removal, substantial sink-filling could be expected. Reversing the process and subtracting the processed elevation realization from the original DEM would result in a modified error surface, which, thanks to flat spots produced by sink filling, would exhibit a much stronger autocorrelation. Therefore, although the initial error surface had weak autocorrelation, its effective autocorrelation for the hydrological modeling would be stronger. Thus the covariance structure alternatives can be expected to be more limited for watersheds with gentle terrain. Coupling that observation with the fact that most flow-routing algorithms perform suboptimally in flat spots generated during sink filling leaves little doubt that error surface autocorrelation choices should be made with care and in accordance with the watershed's characteristics.

[36] The drainage network delineated from a single elevation realization is but one out of an infinite number of possible, alternative depictions of a watershed's hydrologic response. As such, it has little chance of a perfect match to the observed network. This is certainly the case for the areas in Figure 1b corresponding to circled areas in 1a. The Monte Carlo framework employed in this study converts the deterministic approach to probabilistic drainage network identification. A cell found to have consistently large ζ values among individual drainage network realizations is, most likely, situated at a path of accumulated flow and has high probability of being a network member. Accumulated flow passing through a cell on a single elevation realization can be an artifact of elevation error. However, if ζ values for the cell are consistently high in all realizations, then topography in the vicinity of the cell is probably well defined, supportive of flow convergence, and host of a drainage pattern robust against elevation errors potentially present. On the other hand, variable ζ values for a cell indicate sensitivity to elevation errors and an uncertain drainage regime, commonly encountered over ambiguous terrain. Note in Figure 6 the larger variability of ζ values over ambiguous terrain than over well-defined topography hosting the subwatershed's perennial stream, especially when DEMON is used in the simulations.

[37] The ability of the proposed methodology to eliminate or at least reduce the influence of gentle terrain elevation artifacts on delineated drainage networks is related to the ratio of the horizontal extent of the artifact over the error surface autocorrelation, the latter being in our case equivalent to the kernel window diameter. As the size of elevation artifacts approaches the kernel window diameter the performance of our method for drainage network delineation for that area should be expected to deteriorate. Therefore it might be beneficial to investigate error surfaces with stronger autocorrelation, within the limits mentioned earlier, at least in an exploratory manner.

[38] Traditional network derivation by flow accumulation (i.e., using only A) with the D8 algorithm is incapable of representing network discontinuities, which occur often in watersheds with gentle terrain (Figure 1a), because of monotonic increase in A. Substituting ζ for flow accumulation, introduces the slope parameter. Network continuity can now be interrupted, but only if there is a significant increase in S along the flow path. As A increases, a larger S increase is required for network interruption. For this reason, discontinuities in networks derived by using the topographic wetness index and D8 flow-routing algorithm on the original DEM or a single elevation realization are rare and involve only the ephemeral network (Figure 1b).

[39] When ζ is calculated with DEMON, a discontinuity can additionally occur where topography supporting flow convergence is succeeded, along the flow direction, by a zone of flow dispersion. DEMON uses DEM-derived aspect estimates to identify a maximum of two stream tubes passing through a cell. Hence it cannot account for flow variability within the portion of the stream tube represented by the cell. Because of that limitation, and given that estimates of aspect over ambiguous terrain exhibit strong autocorrelation (the range of aspect estimates derived from the unperturbed DEM for flow dispersion zones identified with field observations in Barnard subwatershed was very narrow, $<10^\circ$), the horizontal expansion of flow within the dispersion zone is usually underestimated, and predicted network continuity over the dispersion zone is often maintained. When multiple elevation realizations were considered, per cell range of aspect estimates calculated for each realization in the dispersion zones always exceeded 90° for simulation intensity $k > 15$, resulting in drainage network discontinuities for these areas. In contrast, the range of aspect estimates for cells located on areas with well-defined topography, such as those along the perennial stream, remained low, less than 20° even for $k = 75$, thereby producing a continuous network.

[40] As is evident from Figure 6, the length, and in some instances the width, of the identified drainage network is conditioned by choices of percentile value, λ, used. How much "network" is identified on mean topographic wetness index grids, $\overline{Z}_{(k)}$, is a function of the percentile value, λ, used in deriving $\overline{Z}_{(k)\lambda}$. Larger or smaller values than the

appropriate, yet unknown, λ for a watershed will tend to underestimate or overestimate the spatial extent of the drainage network. Experimenting with more than one value might offer interesting insights regarding the positioning of the drainage network.

[41] The fact that improvement in the delineation fidelity of the perennial network on elevation realizations was only marginal, was attributed in this study to better-defined topography in the vicinity of the perennial network; the same might not hold for watersheds with geomorphological characteristics different than those of Barnard Drain. For a 100-m buffer zone around the perennial network in the study subwatershed, it was found that the contour density, expressed as total contour length per unit area, was 1.62 times the subwatershed mean. Similar contour densities were computed for buffers around the blue lines (perennial network) in DLG topo quads for a dozen subwatersheds adjacent to Barnard Drain [*Gatziolis*, 1998]. In gentle terrain watersheds, where the perennial drainage network crosses regions characterized by watershed-average contour density, it is expected that simulation will improve the perennial network delineation accuracy more than marginally.

[42] The method presented for drainage network delineation is purely terrain-based. The influence of other parameters that affect the network, including soil types and land use practices, is assumed to be minimal and uniform across the watershed. As mentioned, variations in soil type and land use in the Barnard Drain subwatershed are small, and the assumption that these uniformly affect the network appears valid. However, in other watersheds, soil type and land use variability may affect network pattern in ways that terrain-based methods cannot effectively represent, even when the influence of ever-present DEM elevation errors is considered.

4. Conclusions

[43] Elevation errors present in DEMs and inferiorities in the performance of algorithms used to extract drainage networks often lead to inaccurate representations of streams, especially in watersheds with gentle terrain. Monte Carlo simulations with alternative DEM realizations produced by adding autocorrelated error surfaces onto a "stock" DEM, show potential for significantly improving the fidelity of extracted drainage networks. By using only available elevation RMSE estimates for USGS DLG files, our approach produced probabilistic network membership estimates for each cell in a watershed. Although improvement in perennial stream representation fidelity was marginal, it was substantial for the ephemeral network. Natural resource management decisions based on deterministic network delineations that are incapable of accounting for the effect of elevation errors in areas with only ephemeral drainage flow are likely to be poor. Better decisions are likely if the effect of terrain uncertainty is quantified by using multiple elevation realizations as was demonstrated here.

[44] The values of some parameters we used, including the autocorrelation of error surfaces and the topographic wetness index critical value for deciding grid cell network membership, were chosen arbitrarily. However, several choices were explored for these parameters, and justification for choices made is presented. Clearly, experimentation in other watersheds would be required to determine suitable parameters that might be generalizable over a range of watershed types.

[45] Accurate delineation of the drainage network will become increasingly critical for resource managers responsible for the health and condition of riparian corridors and the rest of the ecosystem to which such corridors are linked. The success of the method reported here suggests that these objectives can be achieved in an economical and expeditious way, even over vast land areas, by using data that are already publicly available for the entire United States.

References

Agricultural Research Service (2000), TOPAZ, version 3.1, Grazinglands Res. Lab., U. S. Dep. of Agric., El Reno, Okla.

Bailey, T. C., and A. C. Gatrell (1995), *Interactive Spatial Data Analysis*, Longman, Essex, U. K.

Beasely, D. B., L. F. Huggins, and E. J. Monke (1980), ANSWERS: A model for watershed planning, *Trans. ASAE*, *23*(4), 938–944.

Beven, K. J., and M. J. Kirkby (1979), A physically based variable contributing area model of basin hydrology, *Hydrol. Sci. Bull.*, *24*, 43–69.

Bren, L. J. (1995), Aspects of the geometry of riparian buffer strips and its significance to forestry operations, *For. Ecol. Manage.*, *75*(1–3), 1–10.

Burrough, P. A., and R. A. McDonnell (1998), *Principles of Geographical Information Systems*, Oxford Univ. Press, New York.

Carrara, A., G. Bitelli, and R. Carla (1997), Comparison of techniques for generating digital terrain models from contour lines, *Int. J. Geogr. Inf. Sci.*, *11*(5), 473–541.

Costa-Cabral, M. C., and S. Burges (1994), Digital elevation model networks (DEMON): A model of flow over hillslopes for computation of contributing and dispersal areas, *Water Resour. Res.*, *30*(6), 1681–1692.

Cressie, N. (1991), *Statistics for Spatial Data*, John Wiley, Hoboken, N. J.

Eash, D. A. (1994), A geographic information systems procedure to quantify drainage-basin characteristics, *Water Res. Bull.*, *30*, 1–8.

Ehlschlaeger, C. R., A. M. Shortridge, and M. F. Goodchild (1997), Visualizing spatial data uncertainty using animation, *Comput. Geosci.*, *23*, 387–395.

Fairfield, J., and P. Leymarie (1991), Drainage networks from grid digital elevation models, *Water Resour. Res.*, *27*(5), 709–717.

Fisher, P. F. (1991), First experiments in viewshed uncertainty: The accuracy of the viewshed area, *Photogramm. Eng. Remote Sens.*, *57*, 1321–1327.

Fisher, P. F. (1998), Improved modeling of elevation error with Geostatistics, *GeoInformatica*, *2*(3), 215–233.

Fortin, J. P., R. Moussa, C. Bocquillon, and J. P. Villeneuve (1995), HYDROTEL, un modèle hydrologique distribué pouvant bénéficier des données fournies par la télédétections et les systèmes d'information géographique, *Rev. Sci. Eau*, *8*, 97–124.

Gao, J. (1997), Resolution and accuracy of terrain representation by grid DEMs at a micro-scale, *Int. J. Geogr. Inf. Sci.*, *11*(2), 199–212.

Gatziolis, D. (1998), Predicting soil water content from topographic wetness indices in low relief terrain: Validation and evaluation, M. S. thesis, Mich. State Univ., East Lansing.

Goodchild, M. F. (1980), Algorithm 9: Simulation of autocorrelation for aggregate data, *Environ. Plann. A*, (12), 1073–1081.

Goovaerts, P. (1997), *Geostatistics for Natural Resources Evaluation*, Oxford Univ. Press, New York.

Greco, M. (1996), Erosion processes at the hillslope scale, *Hydrol. Processes*, *10*(7), 985–994.

Hammer, R. D., F. J. Young, N. C. Wollenhaupt, T. L. Barney, and T. W. Haitcoate (1995), *Soil Sci. Soc. Am. J.*, *59*, 509–519.

Heuvelink, G. B. M. (1998), *Error Propagation in Environmental Modelling With GIS*, Taylor and Francis, Philadelphia, Pa.

Holmes, K. W., O. A. Chadwick, and P. C. Kyriakidis (2000), Error in a USGS 30-meter digital elevation model and its impact on terrain modeling, *J. Hydrol.*, *233*, 154–173.

Hunter, G. J., and M. F. Goodchild (1997), Modeling the uncertainty of slope and aspect estimates from spatial databases, *Geogr. Anal.*, *29*, 35–49.

Hutchinson, M. F. (1989), A new procedure for gridding elevation and stream line data with automatic removal of spurious sinks, *J. Hydrol.*, *106*, 211–232.

Hutchinson, M. F. (1996), A locally adaptive approach to the interpolation of digital elevation models, paper presented at Third International Conference/Workshop on Integrating GIS and Environmental Modeling,

Santa Fe, New Mexico, Natl. Cent. for Geogr. Inf. and Anal., Santa Barbara, Calif.

Jenson, S. K. (1991), Applications of hydrologic information automatically extracted from digital elevation models, *Hydrol. Processes*, *5*, 31–41.

Kyriakidis, P. C., A. M. Shortridge, and M. F. Goodchild (1999), Geostatistics for conflation and accuracy assessment of digital elevation models, *Int. J. Geogr. Inf. Sci.*, *13*(7), 677–707.

Lagacherie, P., R. Moussa, D. Cormary, and J. Molenat (1996), Effects of DEM data source and sampling pattern on topographical parameters and on a topography-based hydrological model, in *Application of Geographic Information Systems in Hydrology and Water Resources Management*, edited by K. Kovar, pp. 191–199, Int. Assoc. of Hydrol. Sci., Vienna.

Liu, H., and K. C. Jezek (1999), Investigating DEM error patterns by directional variograms and Fourier analysis, *Geogr. Anal.*, *31*(3), 249–266.

Mantoglou, A., and J. L. Wilson (1982), The turning bands method for simulation of random fields using line generation by a spectral method, *Water Resour. Res.*, *18*(5), 1379–1394.

Mark, D. M. (1988), Network models in geomorphology, in *Modelling in Environmental Systems*, edited by M. G. Anderson, pp. 73–97, John Wiley, Hoboken, N. J.

Martz, L. W., and J. Garbrecht (1999), An outlet breaching algorithm for the treatment of closed depressions in a raster DEM, *Comput. Geosci.*, *25*(7), 835–844.

Mejia, J. M., and I. Rodriguez-Iturbe (1974), On the synthesis of random fields sampling from the spectrum: An application to the generation of hydrological spatial processes, *Water Resour. Res.*, *10*(4), 705–712.

Moore, I. D., and J. C. Gallant (1997), Terrain analysis programs for the Environmental Sciences—Grid version, version 6.3, Cent. for Resour. and Environ. Stud., Aust. Natl. Univ., Canberra.

Moran, P. A. P. (1950), Notes on continuous stochastic phenomena, *Biometrika*, *37*, 17–23.

O'Callaghan, J. F., and D. M. Mark (1984), The extraction of drainage networks from digital elevation data, *Comput. Vision Graphics Image Process.*, *28*, 323–344.

Pilotti, M., and B. Bacchi (1997), Distributed evaluation of the contribution of soil erosion to the sediment yield from a watershed, *Earth Surf. Processes Landforms*, *22*(13), 1239–1251.

Pitlick, J. (1994), Relation between peak flows, precipitation, and physiography of five mountainous regions in the western USA, *J. Hydrol.*, *158*, 219–240.

Quinn, P. F., K. J. Beven, and R. Lamb (1995), The ln(a/tanb) index: How to calculate it and how to use it within the TOPMODEL framework, *Hydrol. Processes*, *9*, 161–182.

Strahler, A. N. (1957), Quantitative analysis of watershed geomorphology, *Eos Trans. AGU*, *38*, 913–920.

U.S. Bureau of the Budget (1947), United States National Map accuracy standards, report, Washington, D. C.

U.S. Soil Conservation Service (1979), *Soil Survey of Ingham County, Michigan*, pp. 34–35, U. S. Dep. of Agric., Washington, D. C.

Veregin, H. (1997), The effects of vertical error in digital elevation models on the determination of flow-path direction, *Cartogr. Geogr. Inf. Syst.*, *2*, 67–79.

Walker, J. P., and G. R. Willgoose (1999), On the effect of digital elevation model accuracy on hydrology and geomorphology, *Water Resour. Res.*, *35*(7), 2259–2268.

Wilson, J. P., and J. C. Gallant (2000), *Terrain Analysis, Principles and Applications*, John Wiley, Hoboken, N. J.

J. S. Fried and D. Gatziolis, Pacific Northwest Research Station, USDA Forest Service, Portland Forestry Sciences Laboratory, Portland, OR 97208, USA. (dgatziolis@fs.fed.us)